Journal of Hazardous Materials 484 (2025) 136732

Contents lists available at ScienceDirect

Journal of Hazardous Materials

journal homepage: www.elsevier.com/locate/jhazmat

Using diatom chain length as a bioindicator of heavy-metals contamination in marine environments

Ruqyyah Mushtaq [a], Chiara Gambardella [b], Roberta Miroglio [b], Fabio Novelli [c], Melania Paturzo [d], Andrea Rubano [a,d], Angela Sardo [e], Sergio Balzano [e], Domenico Paparo [a,d,*]

[a] Physics Department "E. Pancini", University Federico II, via Cintia, 80126 Napoli, Italy
[b] Institute for the Study of Anthropic Impact and Sustainability in the Marine Environment, National Research Council, via De Marini 6, 16149 Genova, Italy
[c] Ruhr University Bochum, Universitätsstrasse 150, 44801 Bochum, DE, Germany
[d] CNR-ISASI, Institute of Applied Sciences and Intelligent Systems "E. Caianiello", via Campi Flegrei 34, 80078 Pozzuoli, Italy
[e] Ecosustainable Marine Biotechnology Department, Zoological Station "A. Dohrn" (SZN), via Acton 55, 80133 Napoli, Italy

HIGHLIGHTS

- Toxicity due to lead, chromium, and copper impaired chain formation in almost all diatoms.
- Terahertz (THz) frequencies are responsive to changes in chain length caused by heavy metals.
- Diatom chain length is useful as a bio-indicator for heavy metal monitoring.
- THz Spectroscopy offers a rapid, harmless and sensitive method for in-vivo detection of heavy metal toxicity in diatoms.

GRAPHICAL ABSTRACT

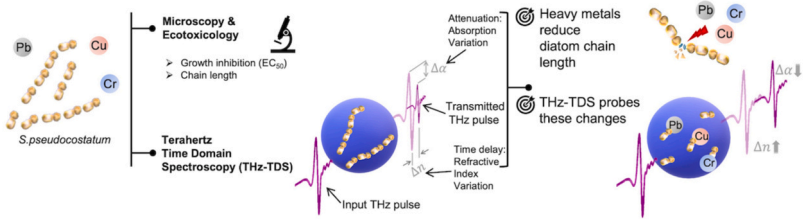

ARTICLE INFO

Keywords:
THz-TDS Spectroscopy
Diatoms
Heavy metal pollution
Marine ecotoxicology

ABSTRACT

The increasing release of toxic heavy metals into marine environments poses significant risks due to their persistence and bioaccumulation. Diatoms are ideal bioindicators because of their sensitivity to environmental changes. Despite traditional methods for detecting these persistent pollutants effectively identify composition and concentration, they are time-consuming, they often require the use of harmful reagents, and do not allow a fast assessment of detrimental impacts on marine organisms. To fill this gap, we have successfully investigated the toxicity of different heavy metals in the marine diatom *Skeletonema pseudocostatum* thanks to a newly developed high-power terahertz (THz) spectrometer. By combining THz spectroscopy, microscopy and ecotoxicological assays, we found that the formation of long diatom chains is significantly inhibited by the presence of lead, copper, and chromium, which disrupt their metabolism. Although the THz absorption and refractive index spectra were not affected by diatom concentration in undoped samples, THz frequencies were highly sensitive to changes in diatom chain length due to heavy metals exposure. These findings suggest that this approach allows to investigate the biochemical processes involved in chain formation in *S. pseudocostatum* and related algae. THz spectroscopy could therefore provide deeper insights into the microscopic metabolic activity of diatoms, addressing key biochemical questions surrounding these organisms. Furthermore, we propose this novel approach for environmental pollution monitoring, since it could provide a rapid, harmless and sensitive detection method to assess heavy metal toxicity in marine diatoms, key organisms at the basis of the trophic chain.

* Corresponding author at: Physics Department "E. Pancini", University Federico II, via Cintia, 80126 Napoli, Italy.
E-mail address: domenico.paparo@cnr.it (D. Paparo).

https://doi.org/10.1016/j.jhazmat.2024.136732
Received 25 July 2024; Received in revised form 22 November 2024; Accepted 30 November 2024
Available online 1 December 2024

1. Introduction

The field of aquatic ecotoxicology has seen significant growth in recent decades due to the exponential increase in chemical production and use in agriculture, medicine, and various industrial sectors. This has led to a rising release of toxic contaminants such as heavy metals, pharmaceuticals, hydrocarbons, pesticides, and plastics into waters globally [1]. Among pollutants, heavy metals pose significant risks to the marine ecological environment due to their widespread sources, difficulty in degradation, bioaccumulation, biomagnification, and long residual times. These metals can have toxic effects on organisms, damaging various tissues and functions upon accumulation [2]. Current aquatic toxicity tests commonly use bioluminescent bacteria [3,4], fleas [5,6], fish [7,8], and algae [9]. These tests usually measure changes in algal biomass [10,11], growth inhibition rates [12], and chlorophyll concentration [13]. However, these techniques are time-consuming (typically $\geq$24 h) [14,15]. Furthermore, structural metrics, including cell counts and biovolume, species composition, and abundance, exhibit high variability. This variation is due to differences among replicates and the diverse distribution across various regions, leading to statistically weak relationships with the studied stressors [14]. Hence, there is an urgent need for methods that are rapid, simple, sensitive, harmless, and robust to test organisms for assessing heavy metal toxicity.

New spectroscopic tools may offer faster and more precise screening capabilities. Techniques like Raman Spectroscopy and Infrared Absorption Spectroscopy are valuable for studying microscopic algae since they are label-free and can be used in-situ [16], though they have limitations [17]. On the one hand, Raman Spectroscopy has a very low efficiency and hence it usually requires a high intensity of light in order to collect a significant signal. It is, thus, difficult to utilize in living systems which are easily damaged by intense laser light. Infrared Spectroscopy on the other hand can access only resonances which are relatively high in energy, and it will thus miss many very important effects and phenomena which are extremely important in biological systems. Emergent vibrational spectroscopies, such as Terahertz Time Domain Spectroscopy (THz-TDS), may circumvent some of these limitations. Terahertz spectroscopy may be considered an extension of Infrared Spectroscopy to the extreme range of the THz frequencies. THz-TDS offers two fundamental advantages over Raman or Infrared Spectroscopy: it is harmless to in vivo organisms and can directly probe the global structural reorganizations of the hydrogen-bond network and the macromolecular vibrational modes of biomolecules [18]. The major drawback of using THz-TDS directly in aqueous environments is the strong absorption of THz radiation by water molecules, which can significantly reduce the THz signal in transmission. Therefore, relatively intense THz sources with a valuable spectral bandwidth are needed for spectroscopic measurements [19]. We emphasize that "intense" in this context still refers to values significantly below the threshold set by Raman spectroscopy, for example, and therefore, it is unable to damage living organisms through heating or ionization.

Diatoms are frequently employed as reference organisms in ecotoxicological research due to their small size, rapid reproduction rate, and sensitivity to environmental shifts [20,21]. Diatoms, part of the Bacillariophyceae class, are microalgae that are nearly ubiquitous in both marine and freshwater ecosystems. In this study we focused on *Skeletonema pseudocostatum*, a centric diatom characterized by radial valve symmetry and commonly found in shallow waters [22], including the coastal waters of the Gulf of Naples. A congeneric species of this diatom serves as useful indicators of marine pollution, being included in international guidelines to assess the toxicity of environmental water samples [23].

Furthermore, *S. pseudocostatum* cells form chains through structures known as "siliceous linking structures" or "mucilage-based junctions." Specifically, these cells are linked via "fused or overlapping silica processes," establishing intercellular bonds [24]. These connections are strengthened by "extracellular mucilage," that stabilizes the chain structure, enabling diatoms to form colonies that offer buoyancy and various ecological advantages. The chain formation is underpinned by highly intricate biochemical processes, that can be affected by natural and human-induced stressors, such as nutrient availability, predation, and contaminants [25–29]. Specifically, changes in diatom chain length have been found after exposure to heavy metals [30]. Copper (Cu), lead (Pb), cadmium (Cd), and mercury (Hg) may interfere with silica deposition process by binding to the organic molecules in the mucilage and causing short chain in marine diatoms.

Based on this observation, we investigated the toxic effects of metals on the chain formation of *S. pseudocostatum* by means of the THz spectroscopy. Our main hypothesis is that specific vibrational collective modes, associated with *S. pseudocostatum* chains, lie within the THz spectral range. Consequently, changes in chain length caused by metal doping may influence the spectral distribution in the THz range, making THz spectroscopy sensitive to the disruption of metabolic processes in diatoms. Furthermore, since the chain formation process may be strongly influenced by diatoms exposure to heavy-metals, we propose monitoring chain formation in *S. pseudocostatum* by means of THz spectroscopy as a new indicator of heavy metal pollution.

THz spectroscopy has been previously applied to investigate the toxic effects of heavy metals on dry samples of *Scenedesmus obliquus*, a species that, like *S. pseudocostatum*, forms chains [31]. This technique demonstrated a faster detection of heavy metals in diatoms compared to conventional methods, but it still required the extraction of large quantities of diatoms, presenting significant challenges from a practical application standpoint. Moreover, no correlation between the THz spectra and algal chain length has ever been investigated so far. In the present study we fill this gap by applying THz spectroscopy to metal-doping in vivo algal samples at environmental concentrations.

Achieving in-vivo capability at natural concentrations requires intense THz sources suitable for investigating dilute aqueous solutions. In this study, we employed a custom-built THz spectrometer based on optical rectification, capable of analyzing dilute aqueous solutions up to 500 μm thick. While less intense sources could potentially work for thinner and more concentrated samples, they would not allow us to study concentrations similar to those found in natural environments due to low signal-to-noise ratios. Among heavy metals, we have selected copper due to its widespread presence in water and its ability to severely impact primary producers at high concentrations, chromium as industrial contamination source, and lead as a benchmark for highly toxic heavy-metal contaminants [31,32].

In the following, we will demonstrate that THz spectroscopy can effectively investigate the disruptive effects of metal doping on the chain formation of *S. pseudocostatum* in their natural environment, seawater, and at concentrations typically observed in nature. This study aims therefore to provide a basis for developing a rapid and sensitive detection method by combining THz technology, ecotoxicology, and cell biology to assess heavy metal pollution in the marine environment, by analyzing diatoms, at the basis of the marine trophic chain.

2. Materials and methods

2.1. Sample preparation

The marine diatoms *S. pseudocostatum* were isolated from the Sarno River mouth (40.72875 N, 14.466432E, Naples, Italy) using the capillary pipette method [33]. They were identified through 18 s and 28 s rDNA gene analysis [34,35]. Initially, the microalgae (8.5×10^5 cells/mL) were cultured in f/2 medium made with sterile filtered (0.22 μm) natural seawater from the oligotrophic areas of the Gulf of Naples at 20 ± 0.5 °C. They were maintained under artificial light with either a 12–12 h light-dark cycle or continuous illumination at a light intensity of 6000–10,000 lx until reaching the exponential growth phase [36].

2.2. Algal growth inhibition test

Toxicity tests were carried out following a modified version of ISO 10253/2016 [23], using multiwell plates instead of glass flasks [37]. An algal pre-culture was started four days before the test, when the cells from the algal stock culture were added to the growth medium to achieve a cell density higher than 10^6 cells /mL in the exponential growth phase. *S. pseudocostatum* cells were then diluted to reach 10^4 cells/mL and exposed to three different toxicants: potassium dichromate $K_2Cr_2O_7$ at concentrations $\rho = 0$, 0.625, 1.25, 2.5, 5 mg/L; pentahydrate copper sulfate $CuSO_4{\cdot}5\ H_2O$ at concentrations $\rho = 0.062$, 0.125, 0.25, 0.5, 1, 2 mg/L; and lead nitrate $Pb(NO_3)_2$ at concentrations $\rho = 0.1$, 0.5, 2, 4 mg/L. Four replicates were prepared for each dilution, and a control sample (algae without toxicant) was included for each dilution.

After 72 h, the culture growth was stopped using Lugol's solution [38], and algal growth inhibition was assessed by counting the cells with a hemocytometer (Bürker chamber) [39], using an inverted microscope (Leica DMi1, Germany). The percentage reduction of the algae number for each metal concentration compared to the control sample was then calculated. The concentration at which this percentage was 50 % was identified as the half maximal effective concentration (EC_{50}). The EC_{50} is a metric used to determine the concentration of a drug, antibody, or toxicant that elicits a biological response halfway between the baseline and the maximum after a specified exposure time, 72 h in the case of *S. pseudocostatum* [40]. To calculate the EC_{50} factor and their confident limits (95 %) we used a Matlab code [41], based on the Trimmed-Spearman-Karber method [42]. To achieve this goal, algae were counted as single cells regardless of chain length. For instance, in Fig. 1a only three cells are counted, although each one is formed by more than one cell unit.

While assessing the ecotoxicity as described before, differences in cell length were observed between control and heavy metal treated samples. Specifically, diatoms exposed to contaminants showed shorter chains than those in control samples (see Fig. 1b for an example). In terms of ecotoxicological effects, this result could lead to an apparent increase in cell number, which was instead due to the cell chain breaking apart because of doping. Therefore, one might erroneously conclude that the diatoms were healthy and growing, while on the contrary they were stressed and breaking into smaller units. Therefore, we explored the possibility of using chain length as a more precise indicator of the diatom wellbeing state. To do this we also counted the number of units present in each chain.

2.3. TDS-THz experiment

The apparatus for TDS-THz experiments is shown in Fig. 2a. For simplicity, we have omitted some optical components that are not essential for understanding the measurement principle. The input laser source was an amplified titanium sapphire (Ti:Sa) laser that emitted pulses with a duration of ~ 90 fs, with a central wavelength of 790 nm and a total output power of 7 W at 1 kHz repetition rate (Coherent).

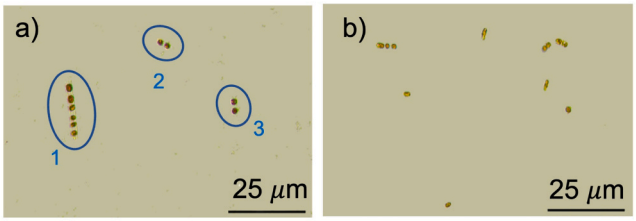

Fig. 1. Microscope images of *Skeletonema pseudocostatum* in a control sample (a) and in a sample doped with 4 mg/L of $(PbNO_3)_2$ toxicant (b). The bar equals 25 μm. Images are collected with an objective with 20× magnification. The blue numbered ellipses enclose each chain, which is counted as one unit in the standard method.

Intense, nearly single-cycle THz pulses were generated via tilted-front optical rectification in a congruent lithium niobate (cLN) prism (MoltTech) [43-46]. The THz power at the sample position, measured by a Gentec THZ12D-3S-VP-D0 detector, was approximately 0.5 mW, equating to 0.5 μJ per pulse. The sample was positioned away from the focus of a parabolic mirror, where the THz beam radius, estimated using an iris, was about 10 mm. At this position, assuming a square pulse, the THz peak field magnitude was around 10 kV/cm.

A small portion of the main beam was transmitted by the beamsplitter and directed to an adjustable delay line for temporal probing of the generated THz pulse using the electro-optic effect in a 1 mm thick ZnTe nonlinear crystal [47]. Fig. 2b-c illustrate the generated THz waveform and corresponding power spectrum. Notably, Fig. 2b shows a signal-to-noise ratio of around 10^5 in the 0.2–1 THz range, which will be the focus of our subsequent analysis.

Diatom solution samples were enclosed in a static liquid cell made of polymethylpentene (TPX) windows and a 0.5 mm thick Teflon spacer to determine the liquid volume under investigation. The cell was maintained at a stabilized temperature of 20.00 ± 0.05 °C. Not shown in Fig. 2a, the setup was enclosed in a nitrogen-purged box to minimize water vapor absorption. In the first set of measurements, THz-TDS experiments were conducted on diatoms at varying concentrations of (0.05, 0.1, 1, 5, 8.5)x10^5 cells/mL. Subsequently, THz spectra were recorded for samples doped with lead nitrate at concentrations of $\rho = 0$, 0.5, 2, 4 mg/L. THz spectra were recorded at the beginning, after 48 h, and, for comparison with the ISO 10253 protocol, after 72 h.

2.4. Absorption coefficient and refractive index extraction

The THz fields $E(t)$ transmitted through the sample are transformed into the frequency domain using Fast Fourier Transform (FFT) to obtain the complex field $E(\nu)$, where ν represents the frequency. By taking the ratio of the FFTs of two THz temporal traces—one with the sample and one without (used as a reference)—the frequency-dependent complex refractive index $\tilde{n}(\nu) = n(\nu) + ik(\nu)$ of the sample can be determined through appropriate analysis. Here, n is the refractive index and k is the extinction coefficient, which is related to the absorption coefficient α by the relation $\alpha = 4\pi k\nu/c$, with c being the speed of light in vacuum.

However, extracting $\tilde{n}(\nu)$ is complicated by Fabry-Pérot reflections that occur at the sample interfaces. In the time domain, these reflections appear as replicas of the initial pulse. The first reflection after the main pulse comes from the interfaces between the output windows of the liquid cell and the sample itself, as indicated by red arrows in Fig. 2d. For clarity, the beam in Fig. 2d is shown as incident at an angle, but in the actual experiment, it impinges the sample at normal incidence. The other main reflections, marked with black-dotted arrows in Fig. 2d, arrive later primarily because the thickness of the cell windows (shown in gray) is much greater than the sample thickness d. The path of the red arrows experiences an additional round-trip time compared to the main pulse, calculated as $2nd/c$, where n is the refractive index of the sample. Assuming a sample thickness of 100 μm and, for simplicity, a refractive index greater than 2.3 for water in the 0.2 – 1 THz range [48], we estimate a delay time of about 1.5 ps. This delay is comparable to the 3 ps wide THz pulse shown in Fig. 2c, making it difficult to distinguish clearly from the main pulse. However, if the cell thickness is increased by a factor of 5, the delay extends to around 7.5 ps. In this case, the main portion of the pulse replica would fall outside the temporal window in Fig. 2c, allowing it to be easily excluded from the analysis. Based on this reasoning, one of the authors showed that the equations for determining changes in the absorption coefficient and refractive index between the sample and the reference can be greatly simplified when working with dilute, very thick samples [49]. Note that this approach is feasible only with very intense THz sources, which provide sufficient signal transmission even in very thick water-based samples.

Under these conditions we have:

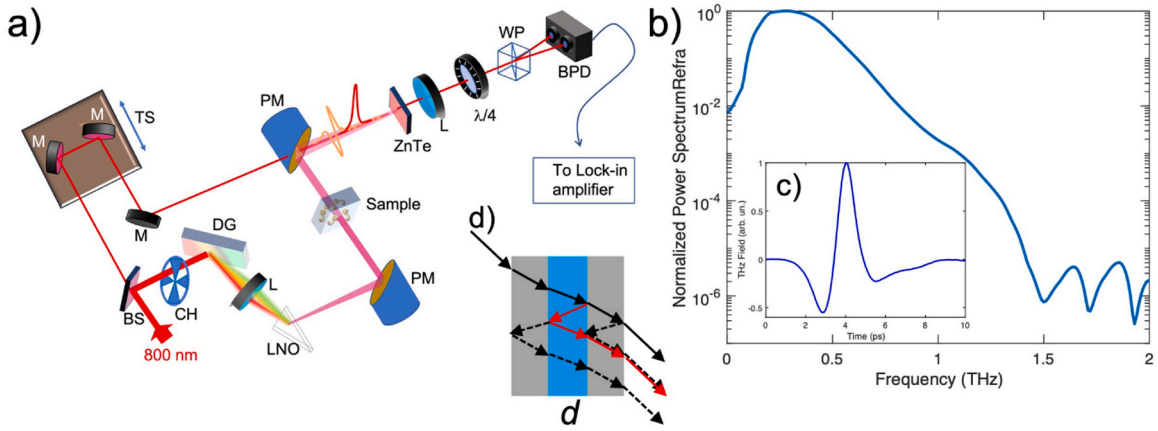

Fig. 2. In panel (a) a scheme of our self-assembled THz spectrometer is shown: BS, 10 % beam-splitter; CH, mechanical chopper; DG, diffraction grating; L, lens; LNO, lithium-niobate crystal; PM, off-axis parabolic mirror; ZnTe, electro-optic crystal; $\lambda/4$, quarter-waveplate; WP, Wollaston prism; BPD, balanced photodiodes; M, mirror; TS, motorized translation stage. In panel (b) the power spectrum of the THz pulse (c) transmitted through a 500 μm thick sample of f/2 medium, mainly water, is shown. The power spectrum is displayed in logarithm scale. (d) Schematic representation of the beam propagation in sample (black arrows) together with Fabry-P é rot reflection (red and black-dotted arrows). Actually, the beam impinges at normal incidence but for clarity it is shown at oblique incidence. The thickness of the cell windows depicted in gray is much larger than the sample thickness *d*.

$$\frac{E_{sol}(\nu)}{E_w(\nu)} = \frac{\tilde{n}_{sol}(\tilde{n}_w + \tilde{n}_{win})^2}{\tilde{n}_w(\tilde{n}_{sol} + \tilde{n}_{win})^2} e^{i\frac{2\pi\nu}{c}\mathrm{d}\Delta n} e^{-\frac{1}{2}\mathrm{d}\Delta\alpha} \tag{1}$$

where $\Delta n = n_{sol} - n_w$ is the frequency-dependent difference between the refraction index of the solution and the solvent, thus f/2 medium in our case; $\Delta\alpha = \alpha_{sol} - \alpha_w$ is the difference of the corresponding absorption coefficients; $\tilde{n}_{win}$ is the complex refractive index of the cell windows.

In the case of dilute solutions, as in our study, we can assume that the prefactor $\tilde{n}_{sol}(\tilde{n}_w + \tilde{n}_{win})^2/\tilde{n}_w(\tilde{n}_{sol} + \tilde{n}_{win})^2$ is approximately equal to one. This leads to the following simplified expressions:

$$\Delta n(\nu) = \frac{c}{2\pi\nu \mathrm{d}} \arg\left[\frac{E_{sol}(\nu)}{E_w(\nu)}\right] \tag{2}$$

$$\Delta\alpha(\nu) = -\frac{2}{\mathrm{d}} \ln\left|\frac{E_{sol}(\nu)}{E_w(\nu)}\right| \tag{3}$$

In summary, performing THz-TDS measurements on a thick aqueous sample involves the following steps: 1. record the two THz fields transmitted by the sample (dilute solution) and reference (ultra-pure milliQ water); 2. perform the FFT on these recorded fields; 3. Take the ratio between the FFT fields; 4. calculate the frequency-dependent phase ($\arg[E_{sol}(\nu)/E_w(\nu)]$) and magnitude ($|E_{sol}(\nu)/E_w(\nu)|$) of this ratio; 5. apply Eqs. 2–3 to calculate the variation of the refractive index and absorption coefficient, respectively.

3. Results and discussion

In this section, we present our findings and elaborate on the key relationships observed between diatom chains and THz spectra, highlighting their significance in developing a novel protocol for detecting heavy metals in marine environments. Initially, we discuss the standard inhibition tests, as outlined in Section 2.2. Traditional standardized tests used in aquatic ecotoxicology [23] consider diatom chains as single uniform units, without accounting for variations in their chain length. This method provides some insights but it does not fully capture the complexity of diatom behavior under metal exposure. We then present measurements using our improved protocol, which diverges from conventional approaches by incorporating differences in diatom chain length. This modification is crucial because chain length may be significantly influenced by the exposure to metal contamination. Considering this factor enhances the accuracy of detecting metal presence and its impact on marine organisms. Finally, we correlate the observed variations in diatom chain length as a function of metal doping with the corresponding changes in THz spectral data.

By following the standard ecotoxicological approach, we measure the percentage reduction in diatom population after 72 h of exposure to various metal concentrations. These results are graphically represented in Fig. 3, where we plot the percentage reduction as a function of the doping levels. A dose-dependent toxicity may be observed for each metal. This dependence allowed us to calculate the EC_{50} values for chromium and copper (Table 1). However, in the case of lead, it is not possible to determine the EC_{50} value since the percentage decrease in the algal population reaches 20 % and remains approximately constant at this level till the highest tested concentration (4 mg/L). This result is in line with the literature, where no ecotoxicological effects have been observed up to these concentrations. The measured toxicity values for chromium and copper (3.7 ± 0.4 mg/L and 1 mg/L, respectively), reported in Table 1, are consistent within the confidence intervals with those available in the literature and/or in the ISO guidelines: 2.5

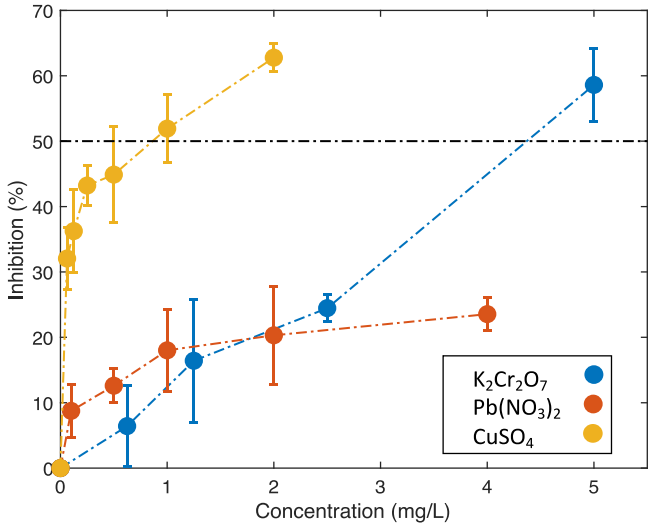

Fig. 3. In the main panel the percentage reduction of the algal population after 72 h is reported for the three different heavy metals. The dashed-dotted lines are only guide for the eyes. The black dashed-dotted line indicates the 50 % level.

Table 1
EC_{50} values as measured in this work (column 2) and found in literature (column 3).

Dopant	EC_{50} (mg/L) and C.L. (95 %) (this work)	EC_{50} (mg/L) and C.L. (95 %) (literature)
$K_2Cr_2O_7$	3.7 ± 0.4	2.5 ± 1.1 [39]
$Pb(NO_3)_2$	NC (> 4 mg/L)	NA
$CuSO_4$	~1 (NC)	1.046 [52]

Note that for copper sulfate the value is not calculable by means of the Trimmed-Spearman-Karber method, but we could provide a graphical estimate by looking at Fig. 3.
NC: not calculable; NA: not available

± 1.1 mg/L [23] and 1.046 mg/L [50], respectively. This result confirms the reliability of our ecotoxicological assays.

After assessing the ecotoxicity of heavy metals, we manually checked the diatom chain length under microscope as a function of doping concentration. We counted the number of individual diatom cells (or units) within each chain and sorted them in a histogram according to the number. The results obtained after the exposure to chromium, copper, and lead are shown in Fig. 4. Note that, to align with the EC_{50} values reported in the literature, in Fig. 3, we have been indicating the concentrations of the salts dissolved in the solution. Now, in Fig. 4, to emphasize the detection limits of the metal alone, we will directly reference the concentration of the metals. Therefore, we will adjust the previous concentrations based on the metal atomic fraction in the salts. For example, the atomic weight of lead (Pb) makes up approximately 62.5 % of the total weight of $Pb(NO_3)_2$. Therefore, a concentration of 0.0101 mg/L of $Pb(NO_3)_2$ corresponds to 0.0063 mg/L of lead alone. This scale adjustment will be reflected in all the graphs dependent on metal concentration that follow.

Notably, in the control sample (not exposed to any toxicant), diatoms could form long chains of up to six units, in agreement with literature [51]. Conversely, in the doped samples, there was a sudden drop in the formation of the longest chains even at the lowest metal concentrations, when chains were mainly formed by one or two cells. Thus, we demonstrated that chain length may be significantly influenced by the exposure to heavy metal contamination, since we found short chains even at the lowest tested concentrations, where no ecotoxicological effects have been observed (see Fig. 3). In particular, by using the traditional ecotoxicological approach based on the EC_{50} value no toxicity is found in marine diatoms exposed to lead, while the new approach proved that this metal affected algal metabolism by reducing chain length in the same way of the other two metals. This result clearly indicates that changes in chain formation in marine diatoms could serve as an alternative and more sensitive factor for monitoring the status of diatoms at an early stage, before irreversible conditions (i.e. mortality) occur.

The results shown in Fig. 4 were obtained by manually counting each individual chain, a time-consuming and imprecise method. Therefore, it is appealing to find an alternative, faster method that is sensitive to the chain length. We will demonstrate in the following that THz-TDS can provide this capability by correlating the variations in diatom chain length as a function of metal doping with the corresponding changes in THz spectral data. Regarding lead, it is important to note that after an initial decrease (Fig. 3), algal population stays roughly constant as the dopant dose increases; this stability allows us to use lead as a reference in the THz-TDS measurements. This way, we can isolate the effect of algal concentration on the THz signal from other factors, such as the hypothesized chain length variation that could cause changes.

Based on these observations, we focus our analysis on the effect of lead on the THz spectra. We start by measuring the THz spectra as a function of the diatom concentration without any dopant. As stated in Section 2.4, we always measure the variation $\Delta\alpha$ of a given sample with respect to an ultra-pure milli-Q water reference. It is important to emphasize that if $\Delta\alpha(\rho_1)$ in medium 1, with a concentration ρ_1 of diatoms or dopant, is greater than $\Delta\alpha(\rho_2)$ in a second medium 2 with concentration ρ_2, this indicates that the sample 1 absorbs more than the sample 2. Conversely, if $\Delta n(\rho_1)$ is greater than $\Delta n(\rho_2)$, the pulse speed in medium 1 will be slower than in medium 2. Therefore, the pulse passing through medium 1 will experience a temporal delay greater than the pulse passing through medium 2.

We display $\Delta\alpha$ for different diatom concentrations and compare them to the absorption of the neat f/2 culture medium in Fig. 5a-b. The insets of panels (a) and (b) show the absolute absorption and refractive index spectra of the culture medium, respectively. From Fig. 5a, it is evident that the absorption spectra show very little variation with diatom concentration and, within the error bars, they perfectly overlap to the spectrum of the f/2 medium. Thus, we may conclude that the absorption spectra of all these samples are equal despite varying the concentration over a large range (0.05–8.5•10^5 cells/mL). Similar conclusions hold for the refractive index spectra in Fig. 5b.

Although the spectra in Fig. 5b are mostly the same within the error margins, some points consistently fall slightly below others. To better explain these data, we have investigated additional parameters able to summarize the integral changes in absorption and refractive index over the whole frequency range we are studying (0.2 to 1 THz). These parameters called "spectral weights" can be measured as follows:

$$W_{\Delta\alpha} = \Delta\nu \sum_i \Delta\alpha(\nu_i) \tag{4}$$

$$W_{\Delta n} = \Delta\nu \sum_i \Delta n(\nu_i) \tag{5}$$

where Σ indicates the summation of all $\Delta\alpha$ and Δn measured at each i-th frequency ν_i and $\Delta\nu \approx 0.07$ THz is the frequency difference between two consecutive points. We also calculate how much these spectral weights change compared to the culture medium (Fig. 5c), by using the following equations:

$$W_{\overline{\Delta\alpha}} = \Delta\nu \sum_i \left[\Delta\alpha - \Delta\alpha_{f/2}\right](\nu_i) \tag{6}$$

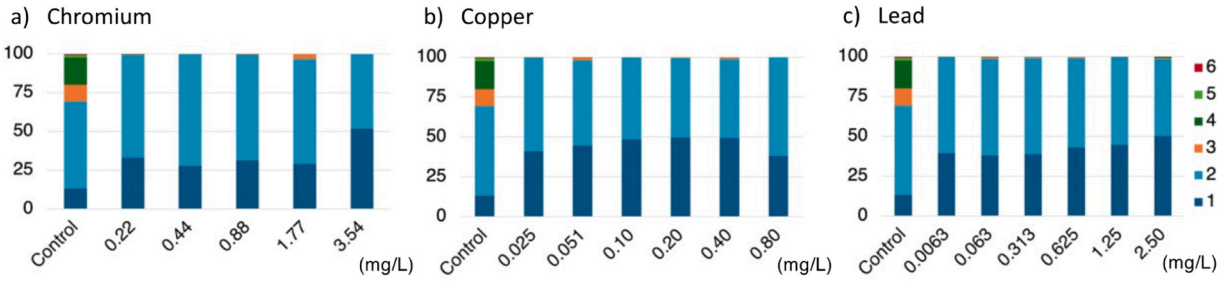

Fig. 4. The histograms illustrate the distribution of chain lengths (expressed in percentage) as a function of the doping level for chromium (a), copper (b), and lead (c). Notably, there is a significant drop in diatoms with chains longer than 2 units even at the lowest doping level. These measurements were taken after 72 h.

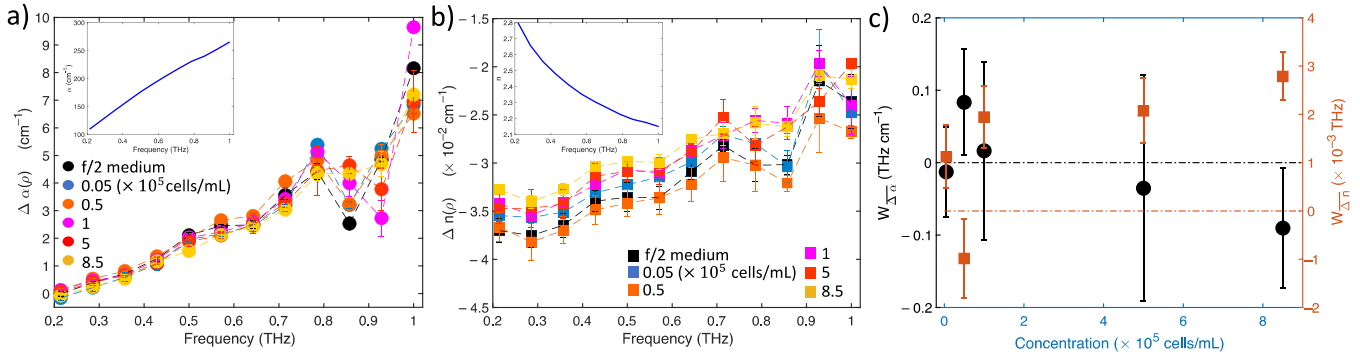

Fig. 5. Variation of the THz absorption (a) and refractive index (b) relative to neat water as a function of cell concentration, without any dopant. In black the data of the pure culture medium f/2 are shown. Dashed lines are a guide to the eye. Panel (c) presents the spectral weight variations compared to the culture medium for different cell concentrations: absorption (black circles) and refractive index (red squares). Insets in panels (a) and (b) show the absorption and refractive index spectra of the culture medium, respectively. The error bars are statistical errors at a 66 % confidence level (one sigma).

$$W_{\overline{\Delta n}} = \Delta\nu \sum_i \left[\Delta n - \Delta n_{f/2}\right](\nu_i) \tag{7}$$

The results show that $W_{\overline{\Delta\alpha}}$ and $W_{\overline{\Delta n}}$ are approximately zero; the absorption $\Delta\alpha$ and the refractive index Δnvariations stay almost constant, meaning that the THz spectra are not significantly affected by how many diatoms are present in the sample.

This result is counterintuitive. To first approximation, the amount of water in the unit volume decreases whenever something is dissolved in it. The solute occupies some space and displaces some water molecules. This is a volume-exclusion effect [52]. As water strongly absorbs THz radiation, the absorption coefficient of an aqueous solution is typically smaller than the one of pure water. In this context, one would expect that increasing the concentration of diatoms would decrease the total absorption compared to that of the f/2 medium. However, our measurements clearly show that this is not the case. One possible reason might be that we do not have sufficient sensitivity to detect this concentration variation. Another explanation could be that the expected decrease in absorption due to the increase in diatom concentration is compensated by the change in the absorption by its hydration water. Alternatively, there could be changes in the absorption characteristics of the diatoms due to their structural modifications. At this stage, we have no evidence for either scenarion, but we will revisit this issue in the following analysis of the THz spectra in the presence of dopants.

The effect of lead on the THz spectra obtained after 48 h and 72 h is shown in Fig. 6. The curves correspond to different doping levels introduced to the samples at the beginning of the experiment (time zero). The spectra at time zero are not shown, as they exhibited no changes, indicating that the dopants require some time before inducing any effects. This is confirmed by Fig. 6a, where we see that $\Delta\alpha$ does not vary after 48 h. The same holds true for Δn in Fig. 6c, although there is a systematic deviation from the other data at a doping level of 4 mg/L. However, we would like to point out that the values remain consistent within the error bars. In contrast, after 72 h, we start to see significant systematic deviations from the control sample, as highlighted in Figs. 6b

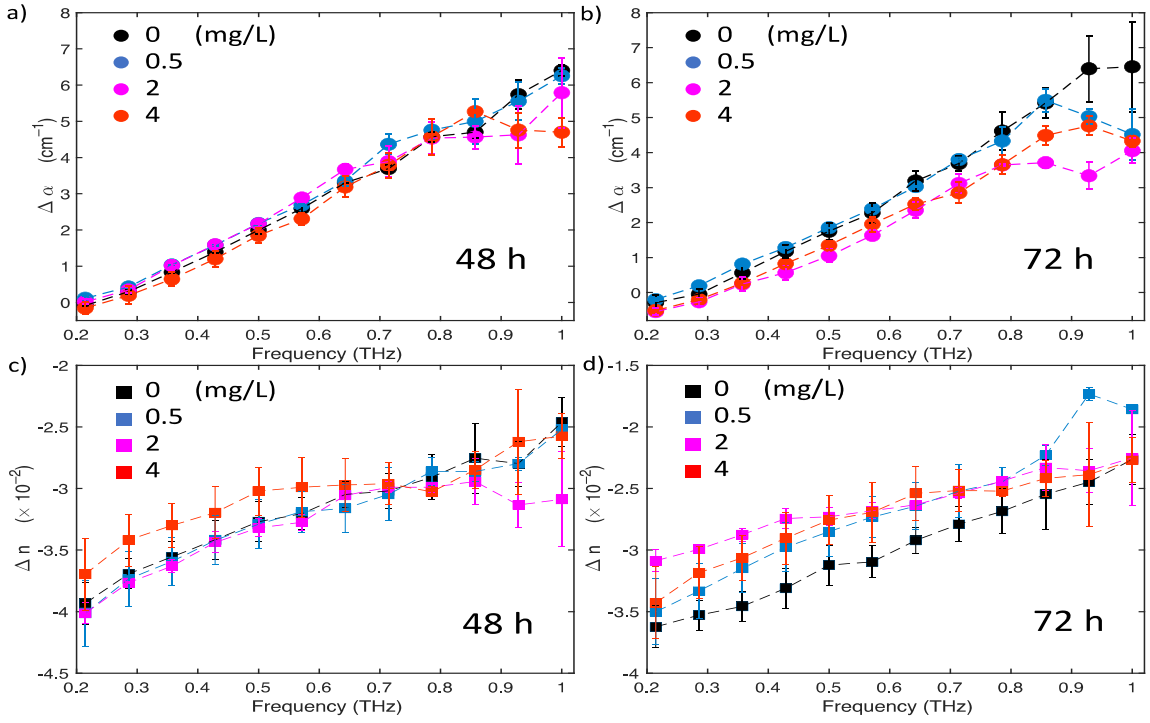

Fig. 6. The variation in THz absorption (a-b) and refractive index (c-d) relative to the culture medium as a function of lead concentration and time. A null concentration represents a control sample with an initial value of 10^4 cells/mL. Errors are shown at a 66 % confidence level. The lines are intended solely as visual aids.

and 6d. Specifically, $\Delta\alpha$ at the highest concentrations is lower than that of the control medium, indicating that the samples with the highest lead concentration are less absorbing compared to the control medium. However, despite being negative, Δn is consistently higher than in the control sample, which implies that the THz pulse at the output of the doped samples experiences a greater delay than at the output of the control medium.

To clarify these findings, we report the absorption spectral weight in Fig. 7a using Eq. 4. To eliminate potential confusion caused by negative values in the refractive index, we consider the magnitude of the spectral weight, denoted as $|W_{\Delta n}|$ and reported in Fig. 7b. The absorption spectral weight for the control sample is almost the same after 48 and 72 h. Although there is some difference in the refractive index spectral weight for the control sample, the values are still quite close when considering measurement errors (Fig. 7b). Both $W_{\Delta\alpha}$ and $|W_{\Delta n}|$ stay nearly constant after 48 h, regardless of doping concentration. However, after a long exposure (72 h), there is a significant change in these values, even at low doping concentrations. We can rule out the possibility that these changes in $W_{\Delta\alpha}$ are due to a decrease in the number of diatoms caused by lead poisoning for three reasons: i) the number of diatoms does not change much with lead doping (Fig. 3); ii) Fig. 5 demonstrates that THz spectra are not greatly affected by the number of diatoms; iii) according to the excluded-volume effect, if the diatom concentration were reduced, we would expect an increase in $\Delta\alpha$, not a decrease. Therefore, we need to consider a different physical mechanism that affects diatom absorptivity, as discussed by Kumar *et al.* [48].

Based on previous results (Fig. 4c), we hypothesize that the changes in the spectral weights $W_{\Delta\alpha}$ and $|W_{\Delta n}|$ might be related to variations in diatom chain length. The length of the diatom chains could affect the vibrational modes or the scattering of THz light, which could impact how much they absorb. To explore this idea, we grouped the diatoms into two categories: those with chain lengths of 2 or single units, and those with 3 or more units. As seen in Fig. 4c, these two groups behave differently when exposed to heavy metals: the first group increases in percentage, becoming almost 100 % of the sample, while the second group almost disappears. We use the data from the histogram in Fig. 4c to estimate the percentage amounts of each group as a function of doping concentration, denoted as $P_{\leq 2}(\rho)$ for the first group and $P_{\geq 3}(\rho)$ for the second one. Since these two groups add up together to 100 %, we know that $P_{\geq 3}(\rho) = 1 - P_{\leq 2}(\rho)$. As the concentration of heavy metals increases, both $W_{\Delta\alpha}$ and $|W_{\Delta n}|$ decrease, which suggests that the spectral weight in the THz range is somehow proportional to $P_{\geq 3}(\rho)$. At this point, we cannot tell exactly which group of diatoms contributes to the THz signal, as we need more information about the vibrations or scattering for each chain length. This can be a possible development of the present work. For now, we focus on the longer chains (3 or more units) and propose the following simple relationships to explain the data:

$$W_{\Delta\alpha}(\rho) = k_{\Delta\alpha} \quad P_{\geq 3}(\rho) \tag{9}$$

$$|W_{\Delta n}(\rho)| = k_{\Delta n} \quad P_{\geq 3}(\rho) \tag{10}$$

where $k_{\Delta\alpha}$ and $k_{\Delta n}$ are two constants, independent on metal concentration.

In Fig. 8 we report the function $P_{\geq 3}(\rho)$ and compare it with $W_{\Delta\alpha}$ and $W_{\Delta n}$. We note that in Fig. 8 $P_{\geq 3}(\rho)$ and $W_{\Delta\alpha}$ have been normalized to their respective maxima and that $|W_{\Delta n}|$ has been further stretched with a factor two. It is remarkable that, except for a scaling factor, both $W_{\Delta\alpha}(\rho)$ and $|W_{\Delta n}(\rho)|$ behave similarly to the curve $P_{\geq 3}(\rho)$as a function of doping concentration and as predicted by Eqs. 9 and 10. Notwithstanding its roughness, this comparison seems to catch the main factor influencing the observed spectral weight variation, supporting the picture that the length of the diatom chain could influence the THz response in this spectral region.

Additionally, we find that the effects of Pb dopant on the growth of diatom chains are detectable at concentrations as low as 0.3 μg/mL using THz-TDS and 6.3 ng/mL using optical microscopy. Although these detection limits are higher than those reported in literature [31], our results are significant because they are achieved in vivo. Furthermore, the abrupt changes previously observed and described (Fig. 4c, Fig. 7b)

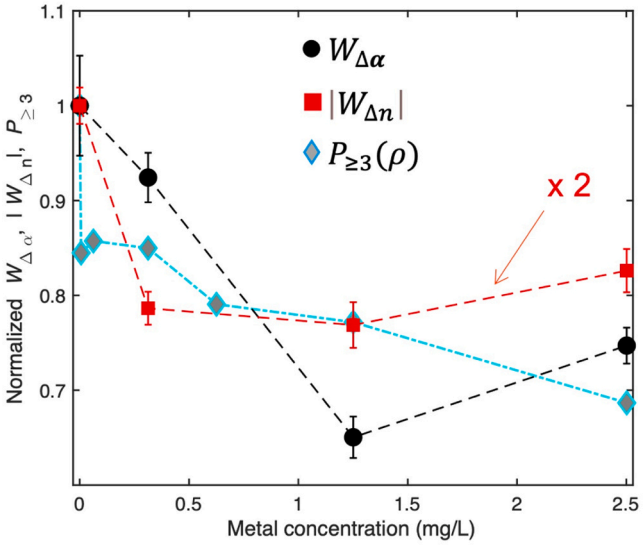

Fig. 8. Normalized absorption spectral weight (black circle), normalized $P_{\geq 3}(\rho)$ distribution (cyan-gray diamonds) and normalized absolute refractive index spectral weight as a function of lead-dopant concentration. Note that the $|W_{\Delta n}|$ curve has been stretched by a factor 2.

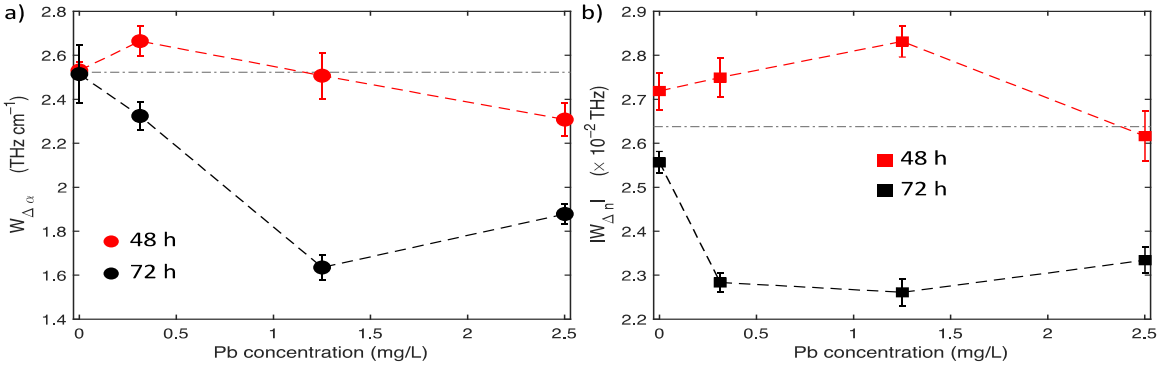

Fig. 7. Absorption spectral weight (a) and refractive index absolute spectral weight (b) as a function of lead dopant concentration after 48 h (red data points) and 72 h (black data point). Error bars indicate a 66 % confidence level. Dashed lines are intended only as visual aids. The horizontal dot-dashed lines indicate the mean of the values at zero concentration of dopant (control sample) after 48 and 72 h.

suggest that these detection limits might be reduced further. To this aim, we plan to conduct more systematic investigations at concentrations lower than those tested in this study. We also observed that the impact on chain formation quickly reaches saturation above the lowest dopant concentrations used, meaning that most diatom chains are affected even at minimal dopant levels. This is a limitation of our technique, as it results in a very reduced dynamic range. Another limitation of the technique is that the effect of metal doping on chain formation requires an extended exposure period (at least 72 h) to become apparent, as demonstrated in Fig. 6 by comparing the spectra at 48 and 72 h. This limitation restricts the technique's suitability for real-time monitoring.

4. Conclusions

We developed and assessed an innovative approach to investigate heavy metal contamination in marine diatoms, which improves both the accuracy and sensitivity in detecting metals and their toxic effects on primary producers at the basis of the marine trophic chain. Specifically, we focused on *S. pseudocostatum* and its ability to self-assemble into chains, demonstrating that chain length might serve as a more precise indicator of algal health than traditional responses, for instance growth. Standard ecotoxicological approaches typically treat each chain as a single unit, neglecting the actual number of cells within each chain. As a result, algae could be classified as healthy even if metal exposure had impaired their ability to form longer chains. In contrast, the ability to form long chains serves as a more reliable indicator of algal wellbeing, particularly in the early stages of contamination.

Moreover, we succeeded in developing a faster method by using a novel THz spectrometer, which allows direct analysis of diatoms in their natural seawater environment, with sensitivity high enough to detect concentrations typical of natural settings. This is a challenging task due to the strong absorption of THz radiation in aqueous solutions. By combining optical microscopy with THz Time-Domain Spectroscopy we discovered that the absorption and refractive index spectra in the THz frequency range are not particularly sensitive to diatom concentrations in undoped samples. However, we found that THz frequencies are highly responsive to variations in diatom chain length caused by heavy metals. This is likely because THz spectroscopy probes specific collective vibrational modes, which are naturally influenced by the chain length, or by changes in the THz scattering cross section, given the comparable dimensions of the diatom chains to THz wavelengths.

To further investigate this hypothesis, we are conducting coarse-grained simulations to link the spectral features observed in the THz range with the specific biochemical processes involved in chain formation. This research could provide THz spectroscopy with the potential to delve deeper into the microscopic metabolic activity of diatoms, answering key questions about the biochemistry of these complex and fascinating systems. Further studies aimed at assessing the impact of other stressors—such as pesticides, pharmaceuticals, other heavy metals, microplastics, etc.—on chain formation will be conducted to verify the application of THz spectroscopy towards a wide range of contaminants.

In conclusion, we verified that specific collective modes associated with the chains of *S. pseudocostatum* lie within the THz spectral range. We highlight that this is the first time that THz spectroscopy has been proven to be sensitive to the chain length of algae in vivo samples. By combining optical microscopy with THz spectroscopy, we demonstrated that chain growth inhibition in *S. pseudocostatum* can serve as a novel indicator for monitoring heavy metal pollution in the marine environment. Notwithstanding the highlighted limitations, the novel approach proposed in this study, based on THz spectroscopy, offers a rapid, harmless and sensitive method to detect heavy metal toxicity in diatoms that should be further considered for monitoring of marine pollution.

Environmental implication

Our study addresses the significant risks of heavy-metal pollution in marine environments due to sources that are widespread, and to the fact that heavy metals degrade slowly, bioaccumulate, biomagnify, and have long residual times. Diatoms, particularly *Skeletonema pseudocostatum*, are ideal bioindicators for these pollutants due to their environmental sensitivity and rapid reproduction. Traditional methods are slow and variable, hindering standardization. We propose a novel method using an intrinsic bioindicator from *S. pseudocostatum*, offering advantages such as in-vivo application and low sample volume requirements, improving the detection of heavy metal pollutants in marine ecosystems.

Funding

PON "Ricerca e Innovazione" 2014-2020, Asse IV "Istruzione e ricerca per il recupero", Azione IV.4 "Dottorati e contratti di ricerca su tematiche dell'innovazione" and Azione IV.5 "Dottorati su tematiche green". FN acknowledges funding by the Deutsche Forschungsgemeinschaft (DFG) under the Individual Research Grant scheme, project 509442914.

CRediT authorship contribution statement

Chiara Gambardella: Writing – review & editing, Validation, Supervision, Resources, Methodology, Investigation, Formal analysis, Data curation, Conceptualization. **Fabio Novelli:** Writing – review & editing, Validation, Supervision, Resources, Methodology, Investigation, Funding acquisition, Data curation, Conceptualization. **Roberta Miroglio:** Writing – review & editing, Validation, Investigation, Data curation. **Andrea Rubano:** Writing – review & editing, Validation, Supervision, Resources, Project administration, Methodology, Funding acquisition, Conceptualization. **Melania Paturzo:** Writing – review & editing, Validation, Methodology, Conceptualization. **Sergio Balzano:** Investigation. **Angela Sardo:** Writing – review & editing, Validation, Resources, Investigation. **Domenico Paparo:** Writing – original draft, Visualization, Validation, Supervision, Project administration, Methodology, Funding acquisition, Formal analysis, Data curation, Conceptualization. **Ruqyyah Mushtaq:** Writing – review & editing, Validation, Investigation, Formal analysis, Data curation.

Declaration of Competing Interest

The authors declare the following financial interests/personal relationships which may be considered as potential competing interests: Ruqyyah Mushtaq reports financial support was provided by Italian Ministry of University and Research. Fabio Novelli reports financial support was provided by Deutsche Forschungsgemeinschaft. If there are other authors, they declare that they have no known competing financial interests or personal relationships that could have appeared to influence the work reported in this paper.

Acknowledgements

We thank the staff of Ecotox LDS S.r.l. for their insights into the ecotoxicology of diatoms. We are also indebted to Pietro Amodeo from CNR-ICB for invaluable discussions.

Data Availability

Data will be made available on request.

References

[1] Ceschin, S., Bellini, A., Scalici, M., 2021. Aquatic plants and ecotoxicological assessment in freshwater ecosystems: a review. Environ Sci Pollut Res 28, 4975–4988. https://doi.org/10.1007/s11356-020-11496-3.

[2] Doyi, I., Essumang, D., Gbeddy, G., Dampare, S., Kumassah, E., Saka, D., 2018. Spatial distribution, accumulation and human health risk assessment of heavy metals in soil and groundwater of the Tano Basin, Ghana. Ecotoxicol Environ Saf 165, 540–546. https://doi.org/10.1016/j.ecoenv.2018.09.015.

[3] Masner, P., Javůrková, B., Bláha, L., 2017. Rapid in situ toxicity testing with luminescent bacteria *Photorhabdus luminescens* and *Vibrio fischeri* adapted to a small portable luminometer. Environ Sci Pollut Res 24, 3748–3758. https://doi.org/10.1007/s11356-016-8096-9.

[4] Qambrani, N.A., Hwang, J.-H., Oh, S.-E., 2016. Comparison of chromium III and VI toxicities in water using sulfur-oxidizing bacterial bioassays. Chemosphere 160, 342–348. https://doi.org/10.1016/j.chemosphere.2016.06.090.

[5] Golding, L.A., McKnight, K., Binet, M., Adams, M., Apte, S.C., 2018. Toxicity of dissolved and precipitated forms of barium to a freshwater alga (*Chlorella* sp. 12) and water flea (*Ceriodaphnia dubia*). Environ Toxicol Chem 37 (6), 1632–1642. https://doi.org/10.1002/etc.4107.

[6] Toyota, K., McNabb, N.A., Spyropoulos, D.D., Iguchi, T., Kohno, S., 2017. Toxic effects of chemical dispersant Corexit 9500 on water flea *Daphnia magna*. J Appl Toxicol 37 (2), 201–206. https://doi.org/10.1002/jat.3343.

[7] Castro, M.P., de Moraes, F.R., Fujimoto, R.Y., da Cruz, C., de Andrade Belo, M.A., de Moraes, J.R.E., 2014. Acute toxicity by water containing hexavalent or trivalent chromium in native Brazilian fish, *Piaractus mesopotamicus*: anatomopathological alterations and mortality. Bull Environ Contam Toxicol 92, 213–219. https://doi.org/10.1007/s00128-013-1174-5.

[8] Robidoux, P.Y., Bérubé, V., Leblanc, J., Desrosiers, M., 2018. Assessment of acute and chronic toxicity of unweathered and weathered diluted bitumen to freshwater fish and invertebrates. Ecotoxicol Environ Saf 164, 331–343. https://doi.org/10.1016/j.ecoenv.2018.08.010.

[9] Yan, H., Pan, G., 2002. Toxicity and bioaccumulation of copper in three green microalgal species. Chemosphere 49 (5), 471–476. https://doi.org/10.1016/s0045-6535(02)00285-0.

[10] Ebenezer, V., Ki, J.-S., 2013. Quantification of toxic effects of the herbicide metolachlor on marine microalgae *Ditylum brightwellii* (Bacillariophyceae), *Prorocentrum minimum* (Dinophyceae), and *Tetraselmis suecica* (Chlorophyceae). J Microbiol 51, 136–139. https://doi.org/10.1007/s12275-013-2114-0.

[11] Wanwan, Y., Tang, Z., Zhou, F., Zhang, W., Song, L., 2013. Toxicity studies of tetracycline on *Microcystis aeruginosa* and *Selenastrum capricornutum*. Environ Toxicol Pharmacol 35 (2), 320–324. https://doi.org/10.1016/j.etap.2013.01.006.

[12] Gao, Q.T., Tam, N.F.Y., 2010. Growth, photosynthesis and antioxidant responses of two microalgal species, *Chlorella vulgaris* and *Selenastrum capricornutum*, to nonylphenol stress. Chemosphere 82, 346–354. https://doi.org/10.1016/j.chemosphere.2010.10.010.

[13] Yan, S., Zhou, Q., 2011. Toxic effects of *Hydrilla verticillata* exposed to toluene, ethylbenzene and xylene and safety assessment for protecting aquatic macrophytes. Chemosphere 85 (6), 1088–1094. https://doi.org/10.1016/j.chemosphere.2011.07.040.

[14] Pandey, L.K., Bergey, E.A., Lyu, J., Park, J., Choi, S., Lee, H., et al., 2017. The use of diatoms in ecotoxicology and bioassessment: insights, advances and challenges. Water Res 118, 39–58. https://doi.org/10.1016/j.watres.2017.01.062.

[15] Pinto, R., Mortagua, A., Almeida, S.F.P., Serra, S., Feio, M.J., 2020. Diatom size plasticity at regional and global scales. Limnetica 39 (1), 387–403. https://doi.org/10.23818/limn.39.25.

[16] Heraud, P., Wood, B.R., Beardall, J., Mcnaughton, D., 2007. Probing the influence of the environment on microalgae using infrared and raman spectroscopy. In: Kneipp, K., Aroca, R., Kneipp, H., Wentrup-Byrne, E. (Eds.), New approaches in biomedical spectroscopy, 963. American Chemical Society, pp. 85–106. https://doi.org/10.1021/bk-2007-0963.ch007.

[17] Coat, R., Montalescot, V., Leon, E.S., Kucma, D., Perrier, C., Jubeau, S., et al., 2014. Unravelling the matrix effect of fresh sampled cells for in vivo unbiased FTIR determination of the absolute concentration of total lipid content of microalgae. Brioprocess Biosyst Eng 37, 2175–2187. https://doi.org/10.1007/s00449-014-1194-5.

[18] Tielrooij, K.J., Paparo, D., Piatkowski, L., Bakker, H.J., Bonn, M., 2009. Dielectric relaxation dynamics of water in model membranes probed by terahertz spectroscopy. Biophys J 97 (9), 2484–2492. https://doi.org/10.1016/j.bpj.2009.08.024.

[19] Novelli, F., Guchhait, B., Havenith, M., 2020. Towards intense THz spectroscopy on water: characterization of optical rectification by GaP, OH1, and DSTMS at OPA wavelengths. Materials 13 (6), 1311. https://doi.org/10.3390/ma13061311.

[20] Debelius, B., Forja, J.M., DelValls, Á., Lubian, L.M., 2009. Toxicity and bioaccumulation of copper and lead in five marine microalgae. Ecotoxicol Environ Saf 72 (5), 1503–1513. https://doi.org/10.1016/j.ecoenv.2009.04.006.

[21] Paixao, S.M., Silva, L., Fernandes, A., O'Rourke, K., Mendonça, E., Picado, A., 2008. Performance of a miniaturized algal bioassay in phytotoxicity screening. Ecotoxicology 17, 165–171. https://doi.org/10.1007/s10646-007-0179-4.

[22] Jung, S.W., Yun, S.M., Lee, S.D., Kim, Y.-O., Lee, J.H., 2009. Morphological characteristics of four species in the genus skeletonema in coastal waters of South Korea. Algae 24, 195–203. https://doi.org/10.4490/ALGAE.2009.24.4.195.

[23] ISO International Organization for Standardization, Water Quality-Marine Algal Growth Inhibition Test with Skeletonema costatum and Phaeodactylum tricornutum (2016), ISO 10253–2016.

[24] Hildebrand, M., 2008. Diatoms, biomineralization processes, and genomics. Chem Rev 108, 4855–4874. https://doi.org/10.1021/cr078253z.

[25] Bellingeri, A., Casabianca, S., Capellacci, S., Faleri, C., Paccagnini, E., Lupetti, P., et al., 2020. Impact of polystyrene nanoparticles on marine diatom *Skeletonema marinoi* chain assemblages and consequences on their ecological role in marine ecosystems. Environ Pollut 262, 114268. https://doi.org/10.1016/j.envpol.2020.114268.

[26] Bergkvist, J., Thor, P., Jakobsen, H.H., Wängberg, S.-Å., Selander, E., 2012. Grazer-induced chain length plasticity reduces grazing risk in a marine diatom. Limnol Oceanogr 57, 318–324. https://doi.org/10.4319/lo.2012.57.1.0318.

[27] Bjærke, O., Jonsson, P.R., Alam, A., Selander, E., 2015. Is chain length in phytoplankton regulated to evade predation? J Plankton Res 37, 1110–1119. https://doi.org/10.1093/plankt/fbv076.

[28] Desrosiers, C., Leflaive, J., Eulin, A., Ten-Hage, L., 2013. Bioindicators in marine waters: Benthic diatoms as a tool to assess water quality from eutrophic to oligotrophic coastal ecosystems. Ecol Indic 32, 25–34. https://doi.org/10.1016/j.ecolind.2013.02.021.

[29] Li, D., Liu, C., Leng, P., Wang, X., Feng, J., Liu, J., et al., 2024. A study on the effect of fluorescently stained micro (nano) plastics on the full life history of *Skeletonema costatum*. Chemosphere 364, 143110. https://doi.org/10.1016/j.chemosphere.2024.143110.

[30] Huang, W., Zhou, Y., Zhao, T., Tan, L., Wang, J., 2021. Effects of copper ions and copper nanomaterials on the output of amino acids from marine algae. Prepr Res Sq. https://doi.org/10.21203/rs.3.rs-324563/v1.

[31] Shao, Y., Wang, Y., Zhu, D., Xiong, X., Tian, Z., Balakin, A.V., et al., 2022. Measuring heavy metal ions in water using nature existed microalgae as medium based on terahertz technology. J Hazard Mater 435, 129028. https://doi.org/10.1016/j.jhazmat.2022.129028.

[32] Tiwari, A.K., Orioli, S., De Maio, M., 2019. Assessment of groundwater geochemistry and diffusion of hexavalent chromium contamination in an industrial town of Italy. J Contam Hydrol 225, 103503. https://doi.org/10.1016/j.jconhyd.2019.103503.

[33] Andersen, R.A., Kawachi, M., 2005. Traditional Microalgae Isolation Techniques. In: Andersen, R.A. (Ed.), Algal culturing techniques. Elsevier Inc, pp. 83–100.

[34] Balzano, S., Marie, D., Gourvil, P., Vaulot, D., 2012. Composition of the summer photosynthetic pico and nanoplankton communities in the Beaufort Sea assessed by T-RFLP and sequences of the 18S rRNA gene from flow cytometry sorted samples. ISME J 6 (8), 1480–1498. https://doi.org/10.1038/ismej.2011.213.

[35] Orsini, L., Sarno, D., Procaccini, G., Poletti, R., Dahlmann, J., Montresor, M., 2002. Toxic *Pseudo-nitzschia multistriata* (Bacillariophyceae) from the Gulf of Naples: morphology, toxin analysis and phylogenetic relationships with other *Pseudo-nitzschia* species. Eur J Phycol 37 (2), 247–257. https://doi.org/10.1017/S0967026202003608.

[36] Gambardella, C., Costa, E., Piazza, V., Fabbrocini, A., Magi, E., Faimali, M., et al., 2015. Effect of silver nanoparticles on marine organisms belonging to different trophic levels. Mar Environ Res 111, 41–49. https://doi.org/10.1016/j.marenvres.2015.06.001.

[37] Lukavsky, J., Simmer, J., 2001. Microprocedure for a standard marine algal bioassay (ISO 10253. Arch für Hydrobiol Suppl, Algol Stud 137, 137–147. https://doi.org/10.1127/algol_stud/101/2001/137.

[38] Gambardella, C., Piazza, V., Albentosa, M., Bebianno, M.J., Cardoso, C., Faimali, M., et al., 2019. Microplastics do not affect standard ecotoxicological endpoints in marine unicellular organisms. Mar Pollut Bull 143, 140–143. https://doi.org/10.1016/j.marpolbul.2019.04.055.

[39] Absher, M., 1973. CHAPTER 1- Hemocytometer Counting. In: Kruse, P.F. Jr, Patterson, M.K. Jr (Eds.), Tissue Culture: Methods and Applications. Academic Press, pp. 395–397. https://doi.org/10.1016/B978-0-12-427150-0.50098-X.

[40] Zheng, C., Bertin, R., Froldi, G., 2013. EC_{50} estimation of antioxidant activity in DPPH assay using several statistical programs. Food Chem 138 (1), 414–420. https://doi.org/10.1016/j.foodchem.2012.11.001.

[41] Stone, B., 2024. Trimmed Spearman-Karber method [software]. ⟨https://www.mathworks.com/matlabcentral/fileexchange/28479-trimmed-spearman-karber-method⟩.

[42] Hamilton, M.A., Russo, R.C., Thurston, R.V., 1977. Trimmed Spearman-Karber method for estimating median lethal concentrations in toxicity bioassays. Environ Sci Tech 11 (7), 714–719. https://doi.org/10.1021/es60130a004.

[43] Hebling, J., Yeh, K.-L., Hoffmann, M.C., Bartal, B., Nelson, K.A., 2008. Generation of high-power terahertz pulses by tilted-pulse-front excitation and their application possibilities. B6-B19 J Opt Soc Am B 25 (7). https://doi.org/10.1364/JOSAB.25.0000B6.

[44] Hirori, H., Doi, A., Blanchard, F., 2013. Erratum: Single-cycle terahertz pulses with amplitudes exceeding 1 MV/cm generated by optical rectification in $LiNbO_3$. Appl Phys Lett 103 (25), 259901. https://doi.org/10.1063/1.4854095.

[45] Hirori, H., Doi, A., Blanchard, F., Tanaka, K., 2011. Single-cycle terahertz pulses with amplitude exceeding MV/cm generated by optical rectification in $LiNbO_3$. Appl Phys Lett 98 (9), 091106. https://doi.org/10.1063/1.3560062.

[46] Tóth, G., Polónyi, G., Hebling, J., 2023. Tilted pulse front pumping techniques for efficient terahertz pulse generation. Light Sci Appl 12 (1), 256. https://doi.org/10.1038/s41377-023-01293-1.

[47] Ulbricht, R., Hendry, E., Shan, J., Heinz, T.F., Bonn, M., 2011. Carrier dynamics in semiconductors studied with time-resolved terahertz spectroscopy. Rev Mod Phys 83 (2), 543–586. https://doi.org/10.1103/RevModPhys.83.543.

[48] Kumar, R., Paturzo, M., Sardo, A., Orefice, I., Yu, Q., Rubano, A., et al., 2022. Toxic effect of metal doping on diatoms as probed by broadband terahertz time-domain spectroscopy. Molecules 27 (18), 5897. https://doi.org/10.3390/molecules27185897.

[49] Novelli, F., 2024. 2024. Terahertz spectroscopy of thick and diluted water solutions. Opt Express 32, 11041–11056. https://doi.org/10.1364/OE.510393.
[50] Guntur, Pratiwi, D.C., Pratiwi, N., Yona, D., Respati, D.S., Kasitowati, R.D., Soegianto, A., 2019. Cadmium and copper toxicity test as growth inhibitor of *Skeletonema costatum*. Pollut Res 38, S22–S26. ⟨https://www.researchgate.net/publication/335991567_CADMIUM_AND_COPPER_TOXICITY_TEST_AS_GROWTH_INHIBITOR_OF_SKELETONEMA_COSTATUM⟩.
[51] Castillo, J.A., Meave del Castillo, M.E., Hernández-Becerril, D.U., 1995. Morphology and distribution of species of the diatom genus *Skeletonema* in a tropical coastal lagoon. Eur J Phycol 30, 107–115. https://doi.org/10.1080/09670269500650871.
[52] Nibali, V.C., Havenith, M., 2014. New insights into the role of water in biological function: studying solvated biomolecules using terahertz absorption spectroscopy in conjunction with molecular dynamics simulations. J Am Chem Soc 136, 12800–12807.